

# Close-Packed Arrangements of Flat-On Free-Base Porphyrins Driven by van der Waals Epitaxy

Marcello Campione,<sup>\*</sup> Conor Hogan, Maurizia Palummo, Alberto Bossi, Rossella Yivlialin, and Gianlorenzo Bussetti<sup>\*</sup>



Cite This: *Cryst. Growth Des.* 2020, 20, 7450–7459



Read Online

ACCESS |



Metrics & More

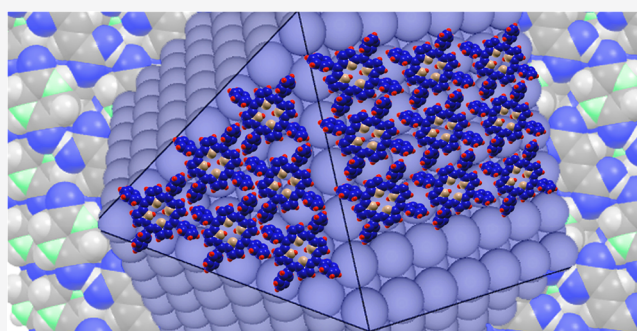


Article Recommendations



Supporting Information

**ABSTRACT:** The functionality of low dimensional phases of porphyrins in optical, chemical, electrical, and multimodal combinational devices is strictly related to the control of molecular orientation within the produced solid layers. A promising strategy to drive the growth of adlayers with predictable structural properties relies on the template effect exerted by the substrate. Tetraphenyl porphyrins, being disc-shaped objects, can be adsorbed on a crystal surface by taking on different geometries. An edge-on configuration is adopted when the interactions among molecules overtake those between molecules and substrate, whereas a flat-on configuration is adopted when molecule-substrate interaction is dominant, with the weaker intermolecular interaction driving a close-packed geometry in the adlayer. For this latter reason, square and/or hexagonal lattice symmetries of physisorbed porphyrin layers are disclosed on highly interacting metal substrates such as Au(111). Unfortunately, metal substrates modify the intrinsic properties of porphyrins by suppressing many of their functionalities. To overcome this drawback, here we report the selective growth of porphyrins in a flat-on arrangement on the chiral (110) cleavage surface of the mixed molecular organic crystal formed by 2,5-diketopiperazine and fumaric acid in a 1:1 mole ratio. The energetic advantage ensured by the interaction with the insulating substrate drives the prevalent formation of domains with a square symmetry, which is retained from monolayer to multilayers. However, rare domains with a hexagonal symmetry are revealed and analyzed by high-resolution scanning probe microscopic techniques. The experimental structural analysis performed at the nanoscale, combined with *ab initio* calculations, allowed us to demonstrate that the molecular architectures we found arise from the simultaneous fulfillment of site adsorption energy maximization driven by peculiar molecular motifs of the selected substrate, close-packing criteria, and epitaxial locking to the substrate surface by weak van der Waals interactions.



## 1. INTRODUCTION

Heterogeneous nucleation is exploited in many branches of solid-state physics and chemistry for promoting and controlling the fabrication of nanostructures. From a thermodynamic point of view, the presence of a foreign surface in a system, where the material to be grown is present at a certain level of concentration, might decrease to a substantial extent the energy barrier for nucleation. The immediate advantage is the possibility to accomplish the material growth at low supersaturation levels, with high rates and with a control on wettability, which is strictly related to the final morphology assumed by the nanostructure. In respect to this last aspect, when molecular materials are deposited, we expect a dependence of the coverage on the molecular orientation. Strategies to select specific orientations and to enhance specific molecular functionalities are based on the ability to find the right trade off between intermolecular interactions and those between molecules and the substrate. Organic epitaxy, in which substrates are surfaces of molecular organic materials

which exert van der Waals (vdW) attraction toward the deposited molecules, has been recently demonstrated effective to drive the ordered growth of various classes of organic materials, from organic semiconductors,<sup>1–6</sup> to biomolecules and organic dielectrics.<sup>7</sup> In addition to the capability, as well as metal surfaces, of templating the growth of organic nanostructures,<sup>8</sup> organic substrates offer the advantage of keeping the intrinsic properties of the deposited material and are electrically insulating. This latter aspect is valuable in the case of a potential integration of the nanostructure in micro/nanoelectronic devices.

**Received:** August 8, 2020

**Revised:** October 14, 2020

**Published:** October 27, 2020



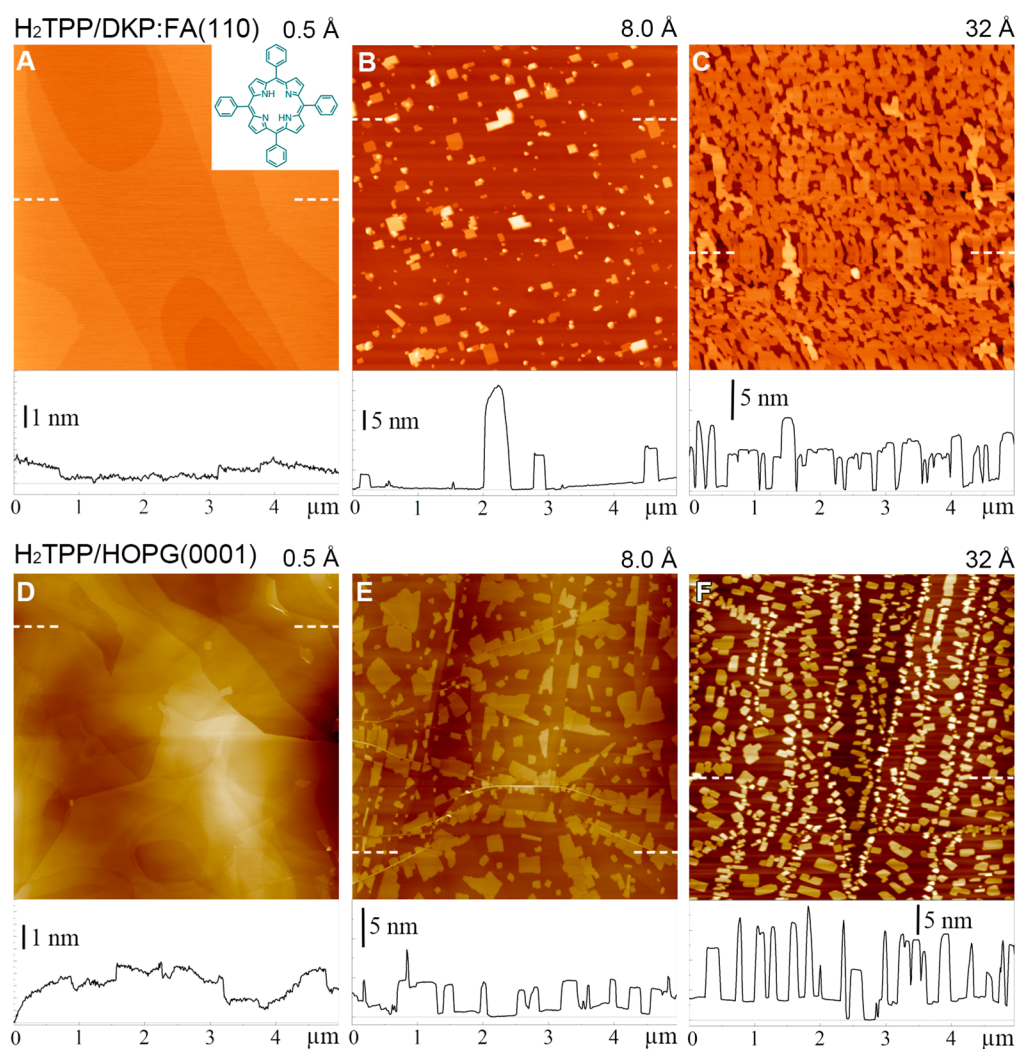


**Figure 1.** Intermittent-contact mode AFM images showing the evolution as a function of the film thickness (ångstroms reported on the top-right of each panel) of H<sub>2</sub>TPP thin films deposited on DKP:FA(110) (A, B, C) and HOPG(0001) (D, E, F). Cross-sectional profiles as taken along the horizontal scan line indicated by the dashed white segments are reported below each image. Panels A and D report the film morphology for nominal thicknesses corresponding to the formation of a wetting layer of H<sub>2</sub>TPP,<sup>29,36</sup> where elemental steps of the cleavage surface of DKP:FA ( $d_{110} = 3.10$  Å) and HOPG ( $d_{0001} = 3.35$  Å) can still be observed. For higher thickness, 3D islands with a height of 5–10 nm decorate the substrate surface.

Within the wide group of porphyrinic compounds, we recognize their technological relevance for their chemical, photochemical, and redox properties, attributable to the presence of the tetrapyrrole core.<sup>9–16</sup> In order to exploit all the functionalities of porphyrin molecules in nanostructures, the most appealing molecular arrangement consists of molecules lying flat on the substrate surface. Under this configuration, being flat molecules, the inner tetrapyrrole core is available to interact with the external environment.

Flat-on arrangements of porphyrins are routinely obtained on metal substrates such as Au,<sup>17–19</sup> Ag,<sup>20–22</sup> Cu,<sup>23–25</sup> and HOPG,<sup>26</sup> but hardly on low interacting surfaces. Recently, we demonstrated the growth of a stable wetting layer of free-base tetraphenyl porphyrin (H<sub>2</sub>TPP; see inset of Figure 1)<sup>27</sup> in a flat-on configuration on an insulating substrate, constituted by the triclinic mixed crystal formed by 2,5-diketopiperazine (DKP) and fumaric acid (FA) in a 1:1 mole ratio (DKP:FA).<sup>28,29</sup> The difficulty of accomplishing this result lies in the absence in H<sub>2</sub>TPP of functional groups promoting strong interactions with the substrate and/or particular in-

plane assemblies.<sup>30,31</sup> Under these conditions, the epitaxial match between substrate and overlayer was demonstrated to be the fundamental driving force enabling the controlled growth of the molecular monolayer. Here, we show by high-resolution atomic force microscopy (AFM) investigations that the flat-on arrangement is retained in crystalline domains of subsequent 3D structures and we disclose the presence of two other epitaxial molecular arrangements. With the help of density functional theory (DFT) calculations, we rationalize such arrangements in terms of close-packed structures arising from the simultaneous occurrence of occupation of preferential substrate sites for nucleation and epitaxial match.

## 2. METHODS

Single crystals of DKP:FA were grown by a slow evaporation at room temperature of 3:1 isopropanol:water solutions. Crystallization time was typically in the range of 1–3 months. Tabular crystals were extracted from the growth vessel and cleaved in air under a stereoscope along the (110) plane with a glaucoma knife. (110)-oriented platelets were glued on a silicon plate and placed in a vacuum chamber. Similarly to other molecular organic crystals and salts, the



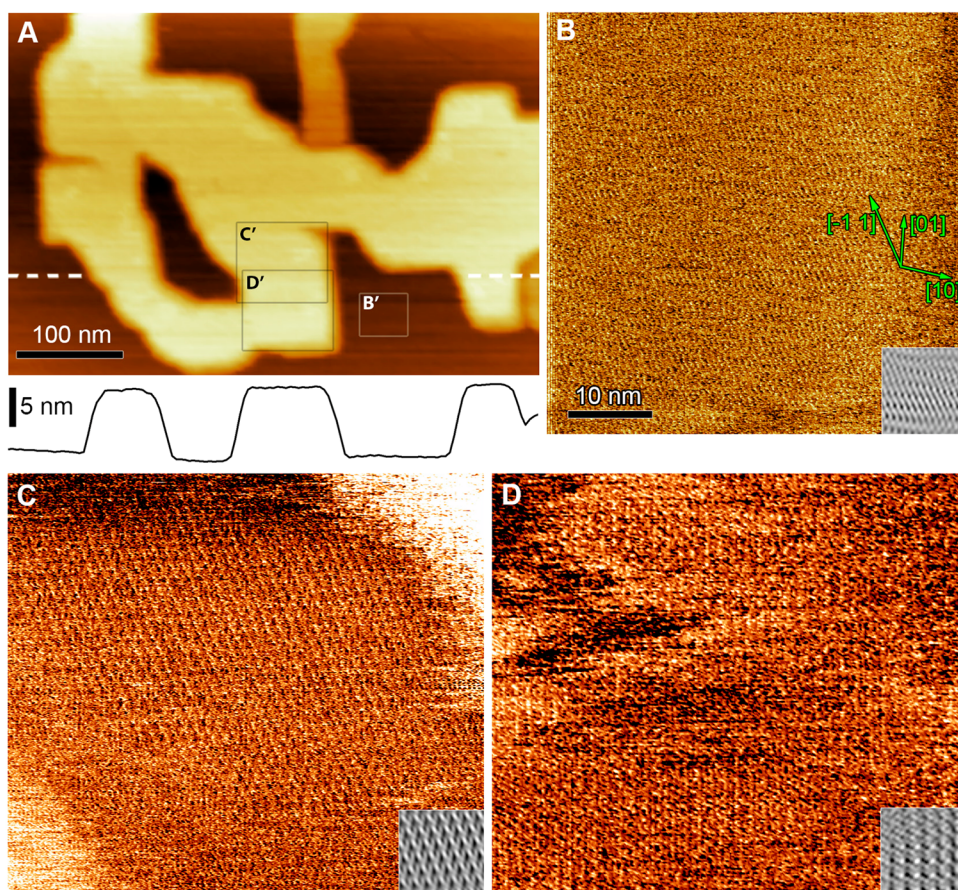


**Figure 2.** (A) Contact-mode AFM image of a 32 Å thick  $\text{H}_2\text{TPP}$  thin film on DKP:FA(110) showing a crystal domain with a thickness of about 10 nm. High-resolution images (friction signal) of the regions highlighted as B', C', and D' are reported in panels B, C, and D, respectively. In (B), the substrate surface corrugation is reported for showing the orientation of the substrate and for evaluating the metrics of film corrugations and epitaxial relations ( $a_1 = 7.30$  Å,  $b_1 = 10.66$  Å,  $\gamma_1 = 101.34^\circ$ ; see Figure 3). In (C) and (D), adjacent hexagonal and square domains are revealed to compose the island reported in (A). The bottom-right inset of each panel shows the Fourier-filtered images for a better visualization of the surface unit cell.

cleavage surface of DKP:FA can be prepared in air and epitaxial growth of other organic overlayers can be accomplished without a cleaning procedure.<sup>5,5</sup> The only transformation we observed on the cleavage surface was some evidence of desorption—giving rise to concave step edges—due to a combined effect of moisture dissolution and re-evaporation. However, this morphological change does not hinder the possibility of epitaxial growth of the organic overlayer.

$\text{H}_2\text{TPP}$  films were grown by physical vapor deposition (PVD) at a pressure of  $5 \times 10^{-7}$  mbar. The sample holder was positioned 300 mm away from the Knudsen cells (K-cell) and was kept at room temperature. The K-cells were thermally controlled via a thermocouple inserted into the crucible.  $\text{H}_2\text{TPP}$  was purchased from Sigma-Aldrich and used as received. Typically, 30 mg of  $\text{H}_2\text{TPP}$  powder was placed inside the K-cell crucible and used for multiple depositions. Under high vacuum (base pressure  $0.5\text{--}1.8 \times 10^{-6}$  mbar), porphyrin was heated at around  $160^\circ\text{C}$  for 1 h and then at a temperature of  $320^\circ\text{C}$  for 10 min. Porphyrin was sublimated on the reference HOPG substrate as well as on the DKP:FA oriented crystals. These latter were glued on a silicon wafer holder;  $\alpha$ -grade HOPG (Optigraph, 1 cm  $\times$  2 cm) was exfoliated with an adhesive tape before the molecule deposition. A quartz microbalance, placed in proximity of the sample, monitored the flux from the cell, allowing one to evaluate the nominal film coverage. Deposition rates were controlled through the K-cell temperatures such that the 0.5 Å thick samples were grown at  $0.06\text{--}0.11$  Å/s rate at a source temperature of ca.  $320^\circ\text{C}$ . The nominal thickness was defined as the final thickness displayed by the quartz crystal microbalance. This was previously calibrated by comparing the nominal thickness of three films with a thickness of the order of tens of nanometers (grown at a constant flux rate of the porphyrin for a

given period of time) with the thickness of the same samples measured *ex situ* by a capacitive profilometer.<sup>13</sup> Due to this calibration, the nominal thickness of 0.5 Å corresponds to an almost complete porphyrin monolayer of roughly 0.5 nm.

The morphological images were collected by using a commercial 5500 Keysight AFM. Intermittent-contact images were acquired using silicon tips (PPP-NCHR, NanoSensors, resonance frequency: ca. 300 kHz, force constant:  $90\text{ N m}^{-1}$ ). The cantilever coating was in aluminum, the tip radius was about 10 nm, and the opening angle was  $40^\circ$ . The cantilever oscillation frequency was set at 0.1 kHz below the resonance, allowing for image acquisition under an attractive regime. Molecular resolution was obtained by using silicon nitride tips mounted on rectangular cantilevers (ORC-8, Bruker, force constant:  $0.05\text{ N m}^{-1}$ ), which is suitable for frictional analysis in contact mode. Molecular-scale friction force images were acquired in both trace and retrace directions with a scan rate of  $8\text{ lines s}^{-1}$ , by minimizing the normal force applied by the tip (set point) to the limit of the disengagement. The image analysis was performed with WSxM software.<sup>32</sup>

Calculations were performed by using DFT in a plane-wave and norm-conserving pseudopotential framework as implemented in the quantum-ESPRESSO code.<sup>33</sup> The PBE exchange-correlation functional<sup>34</sup> was used along with the Grimme D2 semi-empirical vdW correction.<sup>35</sup> The kinetic energy cutoff was 60 Ry. Adsorption of an isolated  $\text{H}_2\text{TPP}$  molecule on DKP:FA(110) was simulated using a single rigid sheet of substrate in a  $3 \times 2$  supercell and an unshifted  $2 \times 2 \times 1$   $k$ -point grid. Geometries were optimized according to a threshold of 12 meV/Å. A small set of initial molecular rotations was considered.

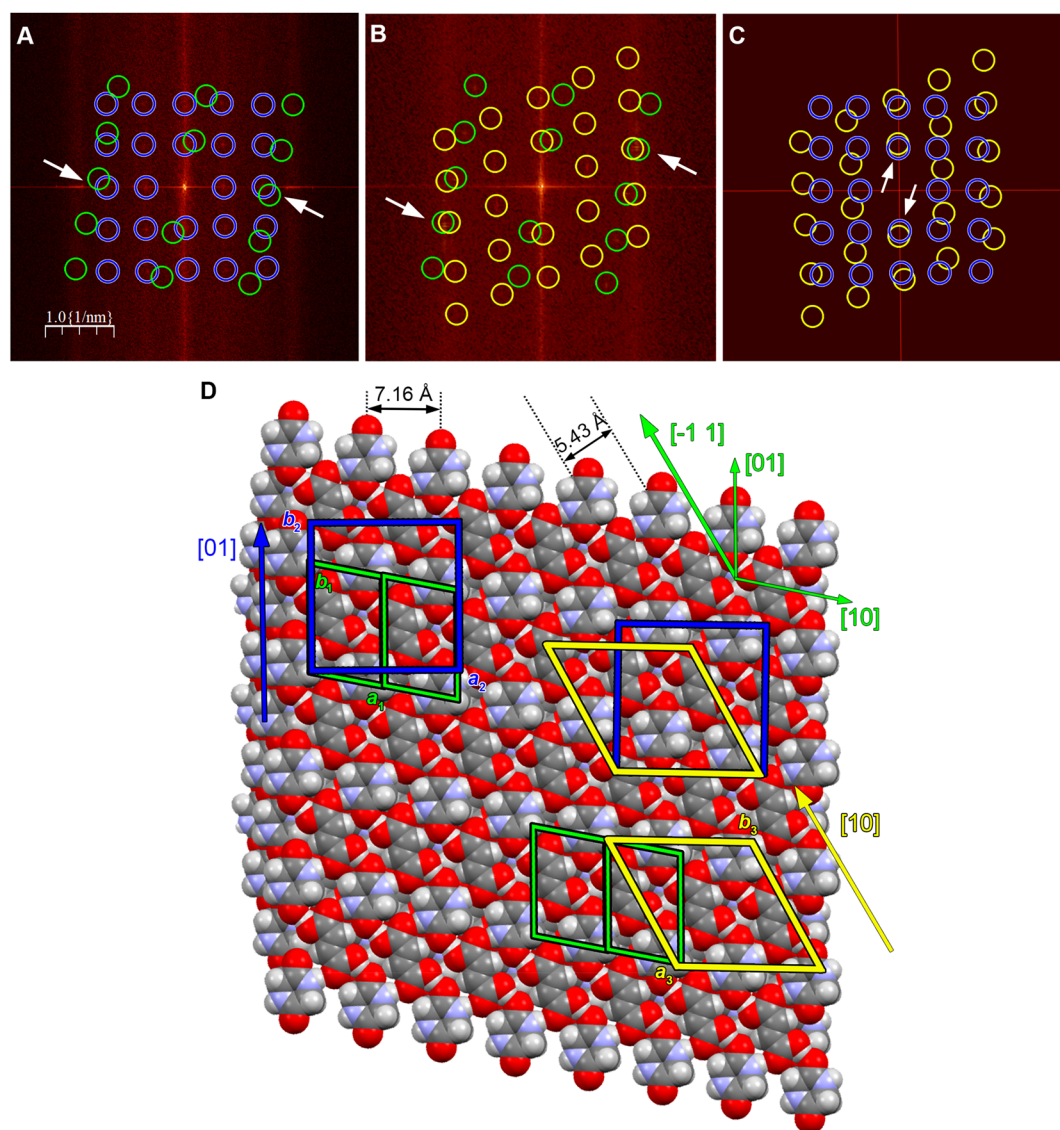


**Figure 3.** (A) Superposition of the 2-D Fourier transforms of the images in parts B and D of Figure 2 highlighting enhanced intensities of the substrate (green circles) and the film (blue circles). The rhombic reciprocal lattice of the substrate and the square reciprocal lattice of the overlayer are clearly identified together with the coincidence (minimum distance between points) of the reciprocal vectors  $H_2TPP_{sq}(20)$  and  $DKP:FA(10)$  (white arrows). (B) Superposition of the 2-D Fourier transforms of the images in parts B and C of Figure 2 highlighting enhanced intensities of the substrate (green circles) and the film (yellow circles). The rhombic reciprocal lattice of the substrate and the hexagonal reciprocal lattice of the overlayer are clearly identified together with the coincidence of the reciprocal vectors  $H_2TPP_{hex}(20)$  and  $DKP:FA(11)$  (white arrows). (C) Superposition of the square and hexagonal reciprocal lattices reported in parts A and B of Figure 2 highlighting enhanced intensities of the  $H_2TPP_{sq}$  (blue circles) and  $H_2TPP_{hex}$  (yellow circles). The coincidence of the reciprocal vectors  $H_2TPP_{sq}(01)$  and  $H_2TPP_{hex}(01)$  is indicated by white arrows. (D) Structural model showing the epitaxial relation deduced from panel A (top-left), implying coincidence between  $H_2TPP(20)$  and  $DKP:FA(10)$  planes and parallelism between  $H_2TPP[01]$  and  $DKP:FA[01]$  directions, panel B (bottom-right), implying coincidence between  $H_2TPP(20)$  and  $DKP:FA(11)$  planes and parallelism between  $H_2TPP[10]$  and  $DKP:FA[-1\ 1]$  directions, and panel C (top-right), implying coincidence between  $H_2TPP_{sq}(01)$  and  $H_2TPP_{hex}(01)$  planes and parallelism between  $H_2TPP_{sq}[10]$  and  $H_2TPP_{hex}[01]$  directions.

Potential energy surfaces (PES) were computed by using a  $1 \times 1$  cell. Benzene was constrained to adsorb in a near-vertical ( $5^\circ$  offset) geometry, while pyrrole was constrained to adsorb in a near-flat (up to  $10^\circ$  rotation) geometry. These offsets allowed a computation of a more realistic PES for adsorption of  $H_2TPP$ . Isolated 2D molecular sheets were studied by using a square and a hexagonal geometry, and a tighter force threshold of 5 meV/Å.

### 3. RESULTS

The morphology evolution as a function of the thickness of  $H_2TPP$  films deposited on  $DKP:FA(110)$  and  $HOPG(0001)$  is shown in Figure 1.

For a nominal thickness of 0.5 Å (Figure 1A,D), molecularly flat terraces separated by steps are clearly visible for both substrates. At this thickness, we demonstrated that  $H_2TPP$  (inset Figure 1A) reaches maximum coverage of its wetting layer, constituted by flat-on molecules with a frozen configuration of their tautomeric form and arranged in a square lattice (Figure S1).<sup>13,29,36</sup> The height of the steps on the surface is within the range 0.3–0.5 nm, consistent with the spacing of elemental steps of the substrates ( $d_{110} = 3.10$  Å for  $DKP:FA$  and  $d_{0001} = 3.35$  Å for  $HOPG$ ) or the thickness of the wetting layer (4.5–5.5 Å). For a nominal thickness higher than 2.0 Å, 3D islands start nucleating and growing up to a height of



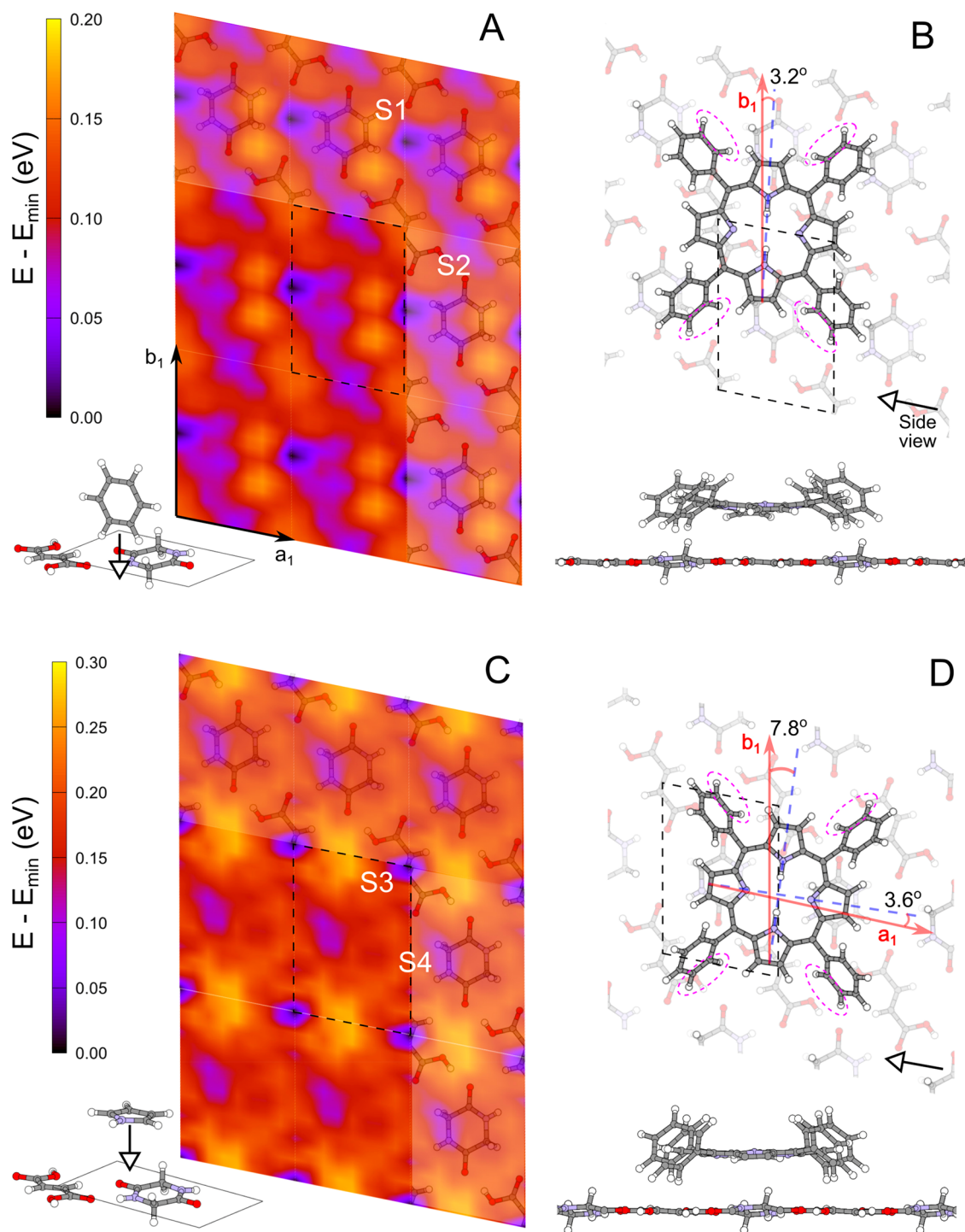


**Figure 4.** (A) Potential energy surface for benzene adsorption on DKP:FA(110). Energies (in eV) are given with respect to the lowest energy site. The substrate unit cell is indicated with dashed lines. The benzene molecule is adsorbed edge-on, with a C–C bond parallel to the substrate plane and to the substrate  $b_1$  axis. The coordinates of the map points indicate the position of the midpoint of the lower C–C bond in benzene. Local minima are indicated as S1 and S2 ( $E_{S1} = E_{S2} - 40$  meV). (B) Accommodation of a  $H_2TPP$  molecule on DKP:FA(110) in a down-buckled conformation enabling occupation of PES minima S1 by all four phenyl rings (atoms closest to the surface are indicated by the pink dashed ovals). The indicated angle is enclosed between the  $b_1$  axis and the molecular axis connecting the midpoints of the C–C bonds of opposite pyrroles (dashed blue line). (C) Potential energy surface for pyrrole adsorption on DKP:FA(110), flat-on. (D) Accommodation of a  $H_2TPP$  molecule on DKP:FA(110) in a flat conformation enabling occupation of S3 and S4 minima by the tetrapyrrole and simultaneously S2 minima (panel B) by the phenyl rings. The indicated angles are enclosed between the  $a_1$  and  $b_1$  axes and the two molecular axes (dashed blue lines).

5–10 nm. At 8.0 Å, the coverage of this 3D phase is 20% for DKP:FA and more than 50% for HOPG (Figure 1B,E, respectively). At 32 Å, the coverage increases and the film morphology changes into a percolation lattice in the case of

DKP:FA (Figure 1C, coverage 90%), while isolated domains are retained in the case of HOPG (Figure 1F, coverage 60%).

To verify the retention of a flat-on arrangement of  $H_2TPP$  in domains grown on DKP:FA, we performed an AFM

investigation on a molecular scale. Figure 2A shows the morphology of a branched microdomain with a thickness of almost 10 nm. High-resolution images were collected on subsequent regions of the same domain. A zoomed image of the area indicated with C' in Figure 2A is reported in Figure 2C, together with a Fourier-filtered image of a  $10 \times 10 \text{ nm}^2$  area as an inset, where a corrugation with a hexagonal symmetry ( $\text{H}_2\text{TPP}_{\text{hex}}$ ) is clearly visible. The hexagonal symmetry of the domain surface extends all over its upper part, whereas, in the lower part, a domain boundary is present, separating a region with a different symmetry. This lower region is indicated with D' in Figure 2A and is reported in Figure 2D, which reveals the presence of an arrangement of molecules with a square symmetry ( $\text{H}_2\text{TPP}_{\text{sq}}$ ) (see also the Fourier-filtered image of a  $10 \times 10 \text{ nm}^2$  area in the inset). The square symmetry was already verified for the epitaxial wetting layer of  $\text{H}_2\text{TPP}$  on DKP:FA;<sup>29</sup> however, the phase visualized in Figure 2D has slight metrical differences with respect to that of the wetting layer and has a different epitaxial relation with the substrate (*vide infra*). On the contrary, the hexagonal phase was detected only on the 3D domains with a frequency lower than 10%.

To allow for the analysis of the epitaxial relation between film phases and substrate surface, we collected a high-resolution image of the bare substrate in a region nearby the  $\text{H}_2\text{TPP}$  domain (region B' in Figure 2A reported in Figure 2B). The surface corrugation is consistent with the bulk-terminated (110) surface having a rhombic lattice with parameters  $a_1 = 7.30 \text{ \AA}$ ,  $b_1 = 10.66 \text{ \AA}$ ,  $\gamma_1 = 101.34^\circ$  (see Figure 3).

To establish the epitaxial match with the  $\text{H}_2\text{TPP}$  overlayer, we performed an analysis in the reciprocal space of the molecular-scale corrugations reported in Figure 2. The output of this analysis is summarized in Figure 3.

The superposition of the 2-D Fourier transforms applied to the images of Figure 2B,D allows putting in evidence the quasi-coincidence of periodicities corresponding to  $\text{H}_2\text{TPP}_{\text{sq}}(20)$  and DKP:FA(10) (Figure 3A). This latter spacing is  $d_{\text{DKP:FA}(10)} = 7.16 \text{ \AA}$ , resulting close to half of the square unit cell parameter of the overlayer ( $a_2 = b_2 = 15.5 \pm 0.8 \text{ \AA}$ ). Under this orientation constraint, the  $\text{H}_2\text{TPP}_{\text{sq}}[01]$  and DKP:FA[01] directions are parallel (Figure 3D, top-left). This epitaxial relation represents a point-on-line coincidence which was predicted on the basis of a tentative  $\text{H}_2\text{TPP}_{\text{sq}}$  phase with  $a_2 = b_2 = 14.3 \text{ \AA}$  but not observed in the wetting layer (see Figure S2 of ref 29). Indeed, the wetting layer of  $\text{H}_2\text{TPP}$  on DKP:FA(110) was observed to have a line-on-line epitaxial relation ensured by a square unit cell with  $\text{H}_2\text{TPP}_{\text{sq}}[01]$  and DKP:FA[01] directions forming an angle of  $4.1^\circ$  and a slightly denser molecular arrangement with  $a_2 = 12.4 \pm 0.8 \text{ \AA}$ ,  $b_2 = 11.2 \pm 0.7 \text{ \AA}$ .<sup>29</sup> The superposition of the 2-D Fourier transforms applied to the images of Figure 2B,C allows putting in evidence the quasi-coincidence of periodicities corresponding to  $\text{H}_2\text{TPP}_{\text{hex}}(20)$  and DKP:FA(11) (Figure 3B). Under this orientation constraint, the  $\text{H}_2\text{TPP}_{\text{hex}}[10]$  and DKP:FA $[-1\ 1]$  directions are parallel (Figure 3D, bottom-right). This epitaxial relation also represents a point-on-line coincidence where the spacing  $d_{\text{DKP:FA}(-1\ 1)} = 5.43 \text{ \AA}$ , results close to half of the spacing  $d_{\text{H}_2\text{TPP}(10)} = 12.8 \pm 0.6 \text{ \AA}$  corresponding to a hexagonal unit cell with parameters  $a_3 = b_3 = 14.8 \pm 0.7 \text{ \AA}$ . Finally, when the reciprocal lattices of  $\text{H}_2\text{TPP}_{\text{sq}}$  and  $\text{H}_2\text{TPP}_{\text{hex}}$

are superimposed (Figure 3C), a clear parallelism of the horizontal parameters is demonstrated (Figure 3D, top-right).

The epitaxial match, while explaining the reciprocal orientation of substrate and overlayer lattices, leaves unresolved the identification of the precise substrate surface sites occupied by the molecules of the overlayer and their orientation. In order to get some quantitative insights into the arrangement of  $\text{H}_2\text{TPP}$  molecules on DKP:FA(110), we performed potential energy surface (PES) calculations on a single rigid DKP:FA(110) sheet. Since a full PES calculation describing the  $\text{H}_2\text{TPP}$  adsorption would be prohibitively expensive due to the molecule's size and floppy nature, we instead looked separately at the adsorption of an edge-on single benzene cycle and of a flat pyrrole ring, respectively. The results, shown in Figure 4, illustrate the competing influence between peripheral phenyl groups and inner tetrapyrrolic cycle on the adsorption site selection.

The PES for a benzene molecule, edge-on aligned with the direction of a C–C bond parallel to the substrate  $b_1$  axis (see Figure 3), is displayed in Figure 4A. The PES shows a clear minimum (S1) lying roughly at the midpoint of the segment connecting two adjacent DKP rings along the  $a_1$  axis. A second local minimum (S2, about 40 meV higher) is found at the corresponding midpoint along the  $a_2$  axis and is connected to S1 by a shallow trough between the chains of DKP and FA molecules along  $[-1\ 1]$ . Maxima occur over the DKP and FA molecules and, in particular, the out-of-plane H atoms bonded to DKP (Figures 4B and 3D).

This calculation suggests that the  $\text{H}_2\text{TPP}$  molecule may be advantageously oriented with its phenyl rings arranged such that they lie as close as possible to the S1 minima. Since the phenyl–phenyl distance ( $\sim 10.5 \text{ \AA}$ ) is close to the DKP:FA  $b_1$ -axis length, this is best achieved if the molecule is oriented with the vertical symmetry axis of the tetrapyrrole ring parallel to  $b_1$ . We thus performed DFT calculations of  $\text{H}_2\text{TPP}$  adsorption on a rigid  $3 \times 2$  supercell of DKP:FA(110) for several orientations and positions compatible with the benzene PES, but allowing the molecule to relax and rotate freely. The optimum configuration obtained after geometry optimization is depicted in Figure 4B, with the corresponding key parameters summarized in Table 1. The final structure is well oriented with respect to the  $b_1$  axis, with the porphyrinic core only misaligned by  $3.2^\circ$ . The average distance between the tetrapyrrole macrocycle and the substrate is  $3.41 \text{ \AA}$ , typical of physisorption, although the lower phenyl H atoms are much closer (see Table 1). The molecule exhibits a noticeable

**Table 1. Adsorption Energy of Isolated  $\text{H}_2\text{TPP}$  on the DKP:FA(110) Substrate from DFT Calculations for Two Possible Geometries<sup>a</sup>**

adsorption energy (eV)	total	vdW component	non-vdW	$d_{\text{min}}$ (Å)	$d_{\text{buckling}}$ (Å)
phenyl-guided (4B)	−2.272	−2.164 (95%)	−0.108 (5%)	1.97	1.45
pyrrole-guided (4D)	−2.426	−2.020 (83%)	−0.406 (17%)	1.75	0.61

<sup>a</sup>The total, defined as  $E_{\text{ads}} = E_{\text{sub}+\text{H}_2\text{TPP}} - E_{\text{sub}} - E_{\text{H}_2\text{TPP}}^{\text{phase}}$ , is split into vdW and non-vdW components.  $E_{\text{sub}}$  and  $E_{\text{H}_2\text{TPP}}^{\text{phase}}$  are the energies of the substrate and isolated molecule.  $d_{\text{min}}$  is the minimum vertical distance between the substrate plane and the molecule;  $d_{\text{buckling}}$  measures the maximum vertical distortion of the (saddle-shaped) porphyrinic core. Energies are in eV.



distortion from planarity: the inner macrocycle becomes saddle-shaped with a maximum out-of-plane extension of 1.45 Å (Figure S2 and Table S2), and the phenyl rings flattened by 23°. The adsorption energy of −2.272 eV is also typical for the physisorption of a large molecule, and indeed 95% of this energy comes from vdW interactions. This value includes an energy penalty of +0.108 eV due to the molecular distortion with respect to the gas phase geometry.

The PES for a single pyrrole ring aligned flat-on is displayed in Figure 4C. There is a clearly favored adsorption site S3 over the midpoint of the FA molecule, and a second favored area S4 over the DKP. The pyrrole PES thus suggests another possible adsorption geometry for the full H<sub>2</sub>TPP molecule that maximizes alignment of the four pyrrole rings over the four S3 and S4 sites. The optimum geometry is shown in Figure 4D. In this orientation, two of the opposite pyrroles (7.15 Å apart) align well with the DKP cycles, separated by 7.30 Å, if H<sub>2</sub>TPP is not buckled and is oriented with its horizontal symmetry axis parallel to *a*<sub>1</sub>. One must note that, under this configuration, phenyl groups are also well aligned with the local S2 minima of the benzene PES (Figure 4D). Thus, this configuration manages to find a good trade off between phenyl adsorption site and pyrrole adsorption site. Although the average distance between the inner tetrapyrrole ring and the substrate is the same as before (3.41 Å), the phenyls are less flattened and their lower H atoms draw closer to the substrate. The porphyrinic core is only weakly buckled (0.6 Å, Figure S2 and Table S2). The adsorption energy of −2.426 eV, still typical of a physisorption, is substantially larger than that of the “phenyl-driven” configuration in Figure 4B. As shown in Table 1, the stronger coupling arises from the significant non-vdW contribution of −0.406 eV. As the energy penalty from strain is about the same as before (+0.096 eV), the larger adsorption energy can thus be traced to the balanced pyrrole-substrate alignment. In contrast, the strong phenyl-S1 interaction in the geometry of Figure 4B leads to a large saddle-shaped distortion of the tetrapyrrolic core, lowering the net non-vdW contribution to −0.108 eV, which is not compensated by the increased vdW interaction.

These calculations establish two favored adsorption geometries of the isolated H<sub>2</sub>TPP molecule. To infer some possible structural models showing the arrangement of H<sub>2</sub>TPP molecules on the top layer of 3D H<sub>2</sub>TPP<sub>sq</sub> and H<sub>2</sub>TPP<sub>hex</sub> domains, we estimated the energy gained in forming a single molecular layer by means of DFT calculations of freestanding 2D sheets of H<sub>2</sub>TPP, as a function of the lattice parameter *a*. For simplicity, the two in-plane lattice parameters are assumed equivalent. The (fixed) 4B and 4D molecular geometries were used in tandem with the square and hexagonal packing orientations observed experimentally. The sheet formation energy for square (sq) packing based on the 4B geometry is  $E_f^{sq,4B} = E_{sheet}^{sq,4B} - E_{H_2TPP}^{4B}$ , where the final term is the energy of an isolated molecule with the 4B geometry; an equivalent expression is used for the other possible geometries.

Results are shown in Figure 5. Formation of a molecular sheet results in a gain of 30–300 meV, depending on the precise geometry and lattice constant. For H<sub>2</sub>TPP<sub>sq</sub>, the 4B and 4D geometries differ in energy by about 40 meV within the experimental range (*a*<sub>2</sub> = *b*<sub>2</sub> = 15.5 ± 0.8 Å), considerably less than the difference between their adsorption energies when considered as single molecules (140 meV). A minimum in the formation energy curve occurs for the 4D geometry at a

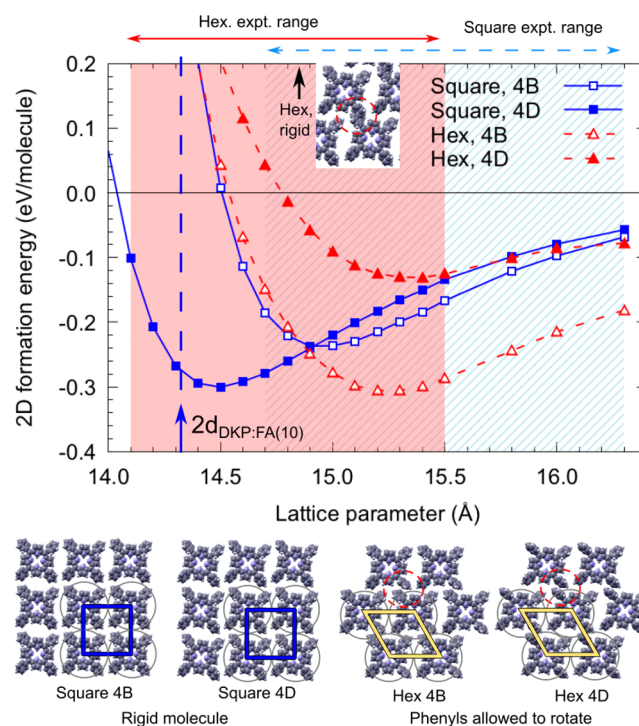


**Figure 5.** Formation energy of 2D sheets of H<sub>2</sub>TPP in square  $E_f^{sq}$  and hexagonal  $E_f^{hex}$  packing conformations. For square lattices, the rigid 4B and 4D molecular geometries are used. Hexagonal packing of rigid molecules is forbidden due to overlap of phenyls (see the inset, top); hence, in this case, they are allowed to rotate (red dashed circles). Energies (in eV) are given with respect to that of a molecule with 4B or 4D geometry. Molecular models for the square and hexagonal surface lattices are drawn by highlighting the similarity with close-packed structure of rigid spheres.

lattice constant close to double the DKP:FA(10) one. The relative stability of the 4D adsorption geometry, coupled with the favorable square packing, suggests this is a good candidate to explain the experimental square phase. H<sub>2</sub>TPP<sub>hex</sub> using fixed geometries is not allowed, however, due to an overlap of adjacent phenyls: if the latter are allowed to rotate, a hexagonal packing can form at the upper range of *a*, but at the expense of an (unknown) energy penalty in the adsorption energy. In this case, the less rotated 4B geometry yields the maximum packing energy. These results are therefore consistent with the rare observation of a hexagonal lattice.

We stress that the actual local molecular geometries within the adsorbed film will differ from the ideal 4B and 4D ones, due to the weak point-on-line coincidence. Nonetheless, typical sheet formation energies are an order of magnitude smaller than the molecular adsorption energies, proving that the molecule–substrate binding is the dominant force driving the adlayer formation.

Note that, in the model of Figure 5, molecules are arranged taking into account the frozen tautomeric form of H<sub>2</sub>TPP.<sup>36</sup> This implies that two molecular orientations rotated by 90° are not energetically equivalent. Therefore, the interaction between the H<sub>2</sub>TPP molecules and the DKA:FA(110) which select a unique domain of the H<sub>2</sub>TPP wetting layer is expected to be retained also in subsequent layers. In the H<sub>2</sub>TPP<sub>hex</sub> configuration, molecules are arranged by considering an isoperimetric transformation of the square lattice with conservation of the vector bases. It is interesting to note that

the relationship between  $H_2TPP_{sq}$  and  $H_2TPP_{hex}$  lattices can be modeled as the result of a plane close-packed arrangement of hard spheres. Indeed, circles with diameters equal to the cell parameter are superimposed on the models of Figure 5. It is evident with this simple analogy that the two structures correspond to those expected by forming square and hexagon close-packed arrangements of hard spheres.

#### 4. DISCUSSION

$H_2TPP$  films deposited on HOPG(0001) and DKP:FA(110) follow a layer-plus-island (Stranski–Krastanov) growth mode, with formation of a one-monolayer-thick wetting layer and subsequent 3D crystalline islands (Figure 1). While a packing with flat-lying molecules is somehow expected and has been demonstrated for the wetting layer, it is not obvious to be retained in 3D islands. Figure 2 proves that a packing with flat-on molecules is also assumed in 3D islands grown on DKP:FA(110). We revealed the presence of two different phases, both epitaxially locked to the substrate through a point-on-line type coincidence but having a different symmetry: a square one and a hexagonal one (Figure 3). We note that the epitaxial wetting layer of  $H_2TPP$  on DKP:FA(110) with square symmetry has a slightly different epitaxial relation with respect to that observed in this work.<sup>29</sup> The square and hexagonal phases of  $H_2TPP$  3D islands on DKP:FA(110) are close-packed structures with a plane unit cell showing an isoperimetric relation with a conservation of the length of the base vectors (Figure 3). To understand this latter relation and to infer the orientation of molecules on substrate site occupation within the overlayers, DFT calculations provide some fruitful hints. The results of Figure 4 indicate that, depending on the competition between peripheral phenyl rings and inner tetrapyrrole in stabilizing  $H_2TPP$  on DKP:FA(110), two orientations of  $H_2TPP$  are predicted: In one orientation, the molecule's symmetry axis is parallel to the substrate  $b_1$  axis and the phenyl rings occupy sites in-between DKP cycles (Figure 4B). In the other orientation, the orthogonal symmetry axis is parallel to the substrate  $a_1$  axis and two pyrrole rings are well overlapped with DKP cycles (Figure 4D), while preserving a favorable accommodation for phenyl rings. The results of DFT calculations show that this latter orientation for the single molecule ensures a maximization (in absolute value) of the adsorption energy. Under this orientation and the geometrical constraints imposed by the experimentally measured lattices, one can build exclusively a monomolecular layer with square symmetry, having the close-packed structure reported in Figure 5. On the other hand, the sole molecular orientation compatible with the observed hexagonal lattice is that one having the vertical molecular axis parallel to  $b_1$  (Figure 5). This molecular orientation cannot take advantage of the pyrrole-DKP interaction, but only of the occupation of S1 sites by phenyl rings (Figure 4B).

Starting from these arguments, we must also take into account that the development of crystal domains is the result of the interplay between local interactions, involving substrate and single  $H_2TPP$  molecules, and collective effects deriving from intermolecular and substrate-overlayer interactions. Local interactions are crucial during the early stages of the layer growth bringing about the formation of a stable nucleus, since molecules are free to diffuse on the substrate surface and are mostly influenced by its interactions. The orientation assumed by a single molecule on the substrate dictates the structure of the overlayer. In our system, isolated molecules can assume

two orientations which generate a square and a hexagonal overlayer, respectively. One must note that, due to the differences in symmetry and metrics between substrate and overlayer lattices, each molecule that adds to the growing overlayer would not always occupy the most favorable site on the substrate. However, this negative effect is compensated by the epitaxial match, through an advantageous interaction deriving from the molecular aggregate as a whole, and by the in-plane molecular aggregation energy. This latter contribution was evaluated to be  $-(30-300)$  meV for the experimentally obtained lattice parameters, *i.e.*, of the order of 1–10% of the molecule-substrate adsorption energy.

We underline that, in accordance with the evaluation of the adsorption energies and substrate-molecule distances (Table 1), the analyzed overlayers, even if apparently influenced by the template effect of the substrate, are only physisorbed. Physisorption explains the spontaneous tendency of aggregates of  $H_2TPP$  on DKP:FA(110) to give rise to plane close-packed arrangements (Figure 5). This means that the square and hexagonal phases might be involved in a homoepitaxial relation, giving rise to alternated layers of different symmetries. On the other hand, the two phases might be involved in an equilibrium state and it would be remarkable to verify in the future that transition from one phase to the other one might be thermally induced.

The results reported here appear somehow in contrast with previous results published on the behavior of  $H_2TPP$  aggregates on a crystalline surface. In particular, contrary to the shown tendency to retain a close-packed arrangement in different phases, low density wetting layers with hexagonal symmetry were reported.<sup>37–39</sup> We note that, besides the results obtained for the in-plane interactions in the isolated 2D  $H_2TPP$  overlayer, also some entropic arguments would support a higher stability of a square symmetry toward a hexagonal one.<sup>40</sup> Accordingly, we revealed very rare domains with hexagonal symmetry, and their existence is ensured by the formation of dense (*i.e.*, close-packed) phases.

#### 5. CONCLUSIONS

In flat-on assemblies of disc-shaped molecules on a surface, it is apparent that substrate-molecule interactions prevail upon intermolecular interactions. Our system comprising  $H_2TPP$  on DKP:FA(110) follows this rule, as substantiated by DFT calculations. However, this simple comparison between in-plane and out-of-plane interactions is not sufficient to account for the occurrence of different symmetries of the overlayer. For a molecule as symmetric as  $H_2TPP$ , it is far more common to reveal molecular monolayers with a square symmetry than a hexagonal one, in contrast with a lower compactness of the former arrangement with respect to the latter. Nonetheless, we identified a peculiar mechanism of selection of this symmetry, driven by the interaction between DKP rings of the substrate surface and pyrrole rings of  $H_2TPP$ . This interaction effectively favors the arrangement of  $H_2TPP$  in such a way that two of its opposite pyrrole rings are aligned along the substrate surface  $a_1$  axis. Additionally, the square packing brings about the formation of a molecular layer epitaxially matched with the substrate, allowing for a further stabilization of the substrate-overlayer interface. The far rarer occurrence of a close-packed hexagonal arrangement of  $H_2TPP$  is justified by the impossibility to retain under this symmetry the beneficial DKP-pyrrole interaction. Nonetheless, also in this case, an



epitaxial coincidence can be accomplished, appearing as a fundamental requirement for stabilizing the H<sub>2</sub>TPP overlayer.

## ■ ASSOCIATED CONTENT

### Supporting Information

The Supporting Information is available free of charge at <https://pubs.acs.org/doi/10.1021/acs.cgd.0c01114>.

Morphological analysis of 0.5 Å thick H<sub>2</sub>TPP films. Adsorption geometry and energy of H<sub>2</sub>TPP on DKP:FA(110) (PDF)

## ■ AUTHOR INFORMATION

### Corresponding Authors

**Marcello Campione** – Department of Earth and Environmental Sciences, Università degli Studi di Milano - Bicocca, I-20126 Milano, Italy; [orcid.org/0000-0001-5627-6186](https://orcid.org/0000-0001-5627-6186); Email: [marcello.campione@unimib.it](mailto:marcello.campione@unimib.it)

**Gianlorenzo Bussetti** – Department of Physics, Politecnico di Milano, I-20133 Milano, Italy; [orcid.org/0000-0001-8556-8014](https://orcid.org/0000-0001-8556-8014); Email: [gianlorenzo.bussetti@polimi.it](mailto:gianlorenzo.bussetti@polimi.it)

### Authors

**Conor Hogan** – Istituto di Struttura della Materia-CNR (ISM-CNR), I-00133 Roma, Italy; Department of Physics, Università di Roma "Tor Vergata", I-00133 Roma, Italy; [orcid.org/0000-0002-0870-6361](https://orcid.org/0000-0002-0870-6361)

**Maurizia Palummo** – Department of Physics and INFN, Università di Roma "Tor Vergata", I-00133 Roma, Italy

**Alberto Bossi** – Istituto di Scienze e Tecnologie Chimiche "G. Natta" of the CNR (CNR-SCITEC), I-20138 Milano, Italy; SmartMatLab Center, I-20133 Milano, Italy

**Rossella Yivlialin** – Department of Physics, Politecnico di Milano, I-20133 Milano, Italy; [orcid.org/0000-0002-6824-1519](https://orcid.org/0000-0002-6824-1519)

Complete contact information is available at: <https://pubs.acs.org/doi/10.1021/acs.cgd.0c01114>

### Notes

The authors declare no competing financial interest.

## ■ ACKNOWLEDGMENTS

M.C. acknowledges the financial support of the University of Milano – Bicocca with FAQC grant no. 2018-ATESP-0010. A.B. thanks Dr. Marta Penconi for the discussion on H<sub>2</sub>TPP film growth and acknowledges the financial support of Progetto Integrato Regione Lombardia and Fondazione CARIPLO (grant nos. 12689/13, 7959/13; Azione 1 e 2, "SmartMatLab centre" and grant 2013-1766). C.H. and M.P. acknowledge high performance computing resources and support from CINECA via the ISCRA initiative.

## ■ REFERENCES

- (1) Raimondo, L.; Fumagalli, E.; Moret, M.; Campione, M.; Borghesi, A.; Sassella, A. Epitaxial Interfaces in Rubrene Thin Film Heterostructures. *J. Phys. Chem. C* **2013**, *117*, 13981–13988.
- (2) Sassella, A.; Campione, M.; Moret, M.; Borghesi, A.; Goletti, C.; Bussetti, G.; Chiaradia, P. Tuning the Growth Mode in Organic Molecular-Beam Epitaxy. *Phys. Rev. B: Condens. Matter Mater. Phys.* **2005**, *71*, 201311.
- (3) Sassella, A.; Campione, M.; Borghesi, A. Organic Epitaxy. *Riv. Nuovo Cimento* **2008**, *31*, 457–490.
- (4) Campione, M.; Raimondo, L.; Moret, M.; Campiglio, P.; Fumagalli, E.; Sassella, A. Organic-Organic Heteroepitaxy of Semi-

conductor Crystals:  $\alpha$ -Quaterthiophene on Rubrene. *Chem. Mater.* **2009**, *21*, 4859–4867.

(5) Campione, M.; Sassella, A.; Moret, M.; Papagni, A.; Trabattini, S.; Resel, R.; Lengyel, O.; Marcon, V.; Raos, G. Organic-Organic Epitaxy of Incommensurate Systems: Quaterthiophene on Potassium Hydrogen Phthalate Single Crystals. *J. Am. Chem. Soc.* **2006**, *128*, 13378–13387.

(6) Koller, G.; Berkebille, S.; Krenn, J. R.; Netzer, F. P.; Oehzelt, M.; Haber, T.; Resel, R.; Ramsey, M. G. Heteroepitaxy of Organic-Organic Nanostructures. *Nano Lett.* **2006**, *6*, 1207–1212.

(7) Evans, P. G.; Spalenka, J. W. Epitaxy of Small Organic Molecules. In *Handbook of Crystal Growth: Thin Films and Epitaxy*, 2nd ed.; Vol. 3; Elsevier Inc., 2015; pp 509–554. DOI: [10.1016/B978-0-444-63304-0.00012-3](https://doi.org/10.1016/B978-0-444-63304-0.00012-3).

(8) Barth, J. V. Molecular Architectonic on Metal Surfaces. *Annu. Rev. Phys. Chem.* **2007**, *58*, 375–407.

(9) De Luca, G.; Romeo, A.; Villari, V.; Micali, N.; Foltran, I.; Foresti, E.; Lesci, I. G.; Roveri, N.; Zuccheri, T.; Scolaro, L. M. Self-Organizing Functional Materials via Ionic Self Assembly: Porphyrins Hand J-Aggregates on Synthetic Chrysotile Nanotubes. *J. Am. Chem. Soc.* **2009**, *131*, 6920–6921.

(10) Monguzzi, A.; Lesci, I. G.; Capitani, G. C.; Santo, N.; Roveri, N.; Campione, M. Mineral-Organic Hybrid Nanotubes as Highly Sensitive Solid State Optical Chemical Sensors. *Phys. Chem. Chem. Phys.* **2014**, *16*, 2491–2498.

(11) Campione, M.; Monguzzi, A.; Santiago-Gonzalez, B.; Villa, C.; Torrente, Y.; Bruzzone, M. G. Composite Functional Nanomaterials Assembled via Electrostatic Interactions of Inorganic Surfaces and Organic Molecules. In *Encyclopedia of Interfacial Chemistry: Surface Science and Electrochemistry*; Elsevier, 2018; pp 32–37. DOI: [10.1016/B978-0-12-409547-2.14137-X](https://doi.org/10.1016/B978-0-12-409547-2.14137-X).

(12) Villa, C.; Campione, M.; Santiago-González, B.; Alessandrini, F.; Erratico, S.; Zucca, I.; Bruzzone, M. G.; Forzenigo, L.; Malatesta, P.; Mauri, M.; Trombetta, E.; Brovelli, S.; Torrente, Y.; Meinardi, F.; Monguzzi, A. Self-Assembled PH-Sensitive Fluoromagnetic Nanotubes as Archetype System for Multimodal Imaging of Brain Cancer. *Adv. Funct. Mater.* **2018**, *28*, 1707582.

(13) Yivlialin, R.; Bussetti, G.; Penconi, M.; Bossi, A.; Ciccacci, F.; Finazzi, M.; Duò, L. Vacuum-Deposited Porphyrin Protective Films on Graphite: Electrochemical Atomic Force Microscopy Investigation during Anion Intercalation. *ACS Appl. Mater. Interfaces* **2017**, *9*, 4100–4105.

(14) Seo, S.; Lee, K.; Min, M.; Cho, Y.; Kim, M.; Lee, H. A Molecular Approach to an Electrocatalytic Hydrogen Evolution Reaction on Single-Layer Graphene. *Nanoscale* **2017**, *9*, 3969–3979.

(15) Vialla, F.; Delpont, G.; Chassagneux, Y.; Roussignol, P.; Lauret, J. S.; Voisin, C. Diameter-Selective Non-Covalent Functionalization of Carbon Nanotubes with Porphyrin Monomers. *Nanoscale* **2016**, *8*, 2326–2332.

(16) Yivlialin, R.; Penconi, M.; Bussetti, G.; Biroli, A. O.; Finazzi, M.; Duò, L.; Bossi, A. Morphological Changes of Porphine Films on Graphite by Perchloric and Phosphoric Electrolytes: An Electrochemical-AFM Study. *Appl. Surf. Sci.* **2018**, *442*, 501–506.

(17) Ruggieri, C.; Rangan, S.; Bartynski, R. A.; Galoppini, E. Zinc(II) Tetrphenylporphyrin Adsorption on Au(111): An Interplay between Molecular Self-Assembly and Surface Stress. *J. Phys. Chem. C* **2015**, *119*, 6101–6110.

(18) Suto, K.; Yoshimoto, S.; Itaya, K. Two-Dimensional Self-Organization of Phthalocyanine and Porphyrin: Dependence on the Crystallographic Orientation of Au. *J. Am. Chem. Soc.* **2003**, *125*, 14976–14977.

(19) Jung, T. A.; Schlittler, R. R.; Gimzewski, J. K. Conformational Identification of Individual Adsorbed Molecules with the STM. *Nature* **1997**, *386*, 696–698.

(20) Yokoyama, T.; Tomita, Y. Central Metal Dependence of Conformation and Self-Assembly of Porphyrins on Ag(110). *J. Chem. Phys.* **2012**, *137*, 244701.

(21) Zotti, L. A.; Teobaldi, G.; Hofer, W. A.; Auwärter, W.; Weber-Bargioni, A.; Barth, J. V. Ab-Initio Calculations and STM

Observations on Tetrapyrrolyl and Fe(II)-Tetrapyrrolyl-Porphyrin Molecules on Ag(111). *Surf. Sci.* **2007**, *601*, 2409–2414.

(22) Auwärter, W.; Seufert, K.; Klappenberger, F.; Reichert, J.; Weber-Bargioni, A.; Verdini, A.; Cvetko, D.; Dell'Angela, M.; Floreano, L.; Cossaro, A.; Bavdek, G.; Morgante, A.; Seitsonen, A. P.; Barth, J. V. Site-Specific Electronic and Geometric Interface Structure of Co-Tetraphenyl-Porphyrin Layers on Ag(111). *Phys. Rev. B: Condens. Matter Mater. Phys.* **2010**, *81*, 245403.

(23) Deng, W.; Fujita, D.; Ohgi, T.; Yokoyama, S.; Kamikado, K.; Mashiko, S. STM-Induced Photon Emission from Self-Assembled Porphyrin Molecules on a Cu(100) Surface. *J. Chem. Phys.* **2002**, *117*, 4995–5000.

(24) Lepper, M.; Köhl, J.; Schmitt, T.; Gurrath, M.; De Siervo, A.; Schneider, M. A.; Steinrück, H. P.; Meyer, B.; Marbach, H.; Hieringer, W. Inverted Porphyrins: A Distorted Adsorption Geometry of Free-Base Porphyrins on Cu(111). *Chem. Commun.* **2017**, *53*, 8207–8210.

(25) Donovan, P.; Robin, A.; Dyer, M. S.; Persson, M.; Raval, R. Unexpected Deformations Induced by Surface Interaction and Chiral Self-Assembly of CoII-Tetraphenylporphyrin (Co-TPP) Adsorbed on Cu(110): A Combined STM and Periodic DFT Study. *Chem. - Eur. J.* **2010**, *16*, 11641–11652.

(26) Chilukuri, B.; Mazur, U.; Hipps, K. W. Effect of Dispersion on Surface Interactions of Cobalt(II) Octaethylporphyrin Monolayer on Au(111) and HOPG(0001) Substrates: A Comparative First Principles Study. *Phys. Chem. Chem. Phys.* **2014**, *16*, 14096–14107.

(27) Gottfried, J. M. Surface Chemistry of Porphyrins and Phthalocyanines. *Surf. Sci. Rep.* **2015**, *70*, 259–379.

(28) Luo, T. J. M.; Palmore, G. T. R. Engineering Crystalline Architecture with Supramolecular Tapes: Studies on Secondary Donor-Acceptor Interactions in Cocrystals of the Cyclic Dipeptide of Glycine. *Cryst. Growth Des.* **2002**, *2*, 337–350.

(29) Campione, M.; Bossi, A.; Yivlialin, R.; Bussetti, G. Uniaxial Alignment of a Monolayer of Flat-on Free-Base Porphyrins on an Exfoliable Insulating Substrate. *Nano Lett.* **2019**, *19*, 5537–5543.

(30) Korolkov, V. V.; Svatek, S. A.; Summerfield, A.; Kerfoot, J.; Yang, L.; Taniguchi, T.; Watanabe, K.; Champness, N. R.; Besley, N. A.; Beton, P. H. Van Der Waals-Induced Chromatic Shifts in Hydrogen-Bonded Two-Dimensional Porphyrin Arrays on Boron Nitride. *ACS Nano* **2015**, *9*, 10347–10355.

(31) Korolkov, V. V.; Baldoni, M.; Watanabe, K.; Taniguchi, T.; Besley, E.; Beton, P. H. Supramolecular Heterostructures Formed by Sequential Epitaxial Deposition of Two-Dimensional Hydrogen-Bonded Arrays. *Nat. Chem.* **2017**, *9*, 1191–1197.

(32) Horcas, I.; Fernández, R.; Gómez-Rodríguez, J. M.; Colchero, J.; Gómez-Herrero, J.; Baro, A. M. WSXM: A Software for Scanning Probe Microscopy and a Tool for Nanotechnology. *Rev. Sci. Instrum.* **2007**, *78*, 013705.

(33) Giannozzi, P.; Andreussi, O.; Brumme, T.; Bunau, O.; Buongiorno Nardelli, M.; Calandra, M.; Car, R.; Cavazzoni, C.; Ceresoli, D.; Cococcioni, M.; Colonna, N.; Carnimeo, I.; Dal Corso, A.; De Gironcoli, S.; Delugas, P.; Distasio, R. A.; Ferretti, A.; Floris, A.; Fratesi, G.; Fugallo, G.; Gebauer, R.; Gerstmann, U.; Giustino, F.; Gorni, T.; Jia, J.; Kawamura, M.; Ko, H. Y.; Kokalj, A.; Küçükbenli, E.; Lazzeri, M.; Marsili, M.; Marzari, N.; Mauri, F.; Nguyen, N. L.; Nguyen, H. V.; Otero-De-La-Roza, A.; Paulatto, L.; Poncè, S.; Rocca, D.; Sabatini, R.; Santra, B.; Schlipf, M.; Seitsonen, A. P.; Smogunov, A.; Timrov, I.; Thonhauser, T.; Umari, P.; Vast, N.; Wu, X.; Baroni, S. Advanced Capabilities for Materials Modelling with Quantum ESPRESSO. *J. Phys.: Condens. Matter* **2017**, *29*, 465901.

(34) Perdew, J. P.; Burke, K.; Ernzerhof, M. Generalized Gradient Approximation Made Simple. *Phys. Rev. Lett.* **1996**, *77*, 3865–3868.

(35) Grimme, S. Semiempirical GGA-Type Density Functional Constructed with a Long-Range Dispersion Correction. *J. Comput. Chem.* **2006**, *27*, 1787–1799.

(36) Bussetti, G.; Campione, M.; Riva, M.; Picone, A.; Raimondo, L.; Ferraro, L.; Hogan, C.; Palummo, M.; Brambilla, A.; Finazzi, M.; Duò, L.; Sassella, A.; Ciccacci, F. Stable Alignment of Tautomers at Room Temperature in Porphyrin 2D Layers. *Adv. Funct. Mater.* **2014**, *24*, 958–963.

(37) Scarselli, M.; Ercolani, G.; Castrucci, P.; Monti, D.; Bussetti, G.; Russo, M.; Goletti, C.; Chiaradia, P.; Paolesse, R.; De Crescenzi, M. A Combined Scanning Tunneling Microscopy and Reflectance Anisotropy Spectroscopy Investigation of Tetraphenylporphyrin Deposited on Graphite. *Surf. Sci.* **2007**, *601*, 2607–2610.

(38) Scarselli, M.; Castrucci, P.; Monti, D.; De Crescenzi, M. Studies of the Adsorption of Tetraphenylporphyrin Molecules on Graphite. *Surf. Sci.* **2007**, *601*, 5526–5532.

(39) Goletti, C. *Optical Anisotropy of Thin and Ultrathin Porphyrin Layers*; Springer: Berlin, 2014. DOI: 10.1007/7081\_2014\_135.

(40) Zangi, R.; Rice, S. A. Hexagonal to Square Lattice Conversion in Bilayer Systems. *Phys. Rev. E: Stat. Phys., Plasmas, Fluids, Relat. Interdiscip. Top.* **2000**, *61*, 671–681.